The in-plane elastic properties of hierarchical composite cellular materials: synergy of hierarchy, material heterogeneity and cell topology at different levels - Appendices

Appendix A. Relation between the Young's modulus of the filling material and the corresponding Winkler foundation constant

As stated in Section 2, the Euler-Bernoulli beam on Winkler foundation model simulates the composite hexagonal microstructure at all levels. Specifically, a sequence of closely spaced independent linear-elastic springs approximates the cells filling material. Note that representing the material within the cells by a Winkler foundation is a simplification to obtain a more mathematically tractable problem. However, notwithstanding the limitations introduced, the analysis in [1] reveals the validity of the modeling approach based on the Winkler model. A suitable relation between the Young's modulus of the filling material, $E_f^{(i)}$ and the Winkler foundation constant, $k_w^{(i)}$, is also provided [1]:

$$E_f^{(i)} = \frac{5\sqrt{3}}{8} K_w^{(i)}, \qquad i = 1, 2, 3, \tag{A.1}$$

been $K_w^{(i)} = k_w^{(i)}\, \ell^{(i)}$ and $\ell^{(i)}$ the length of the cell walls.

Assuming that the material inside the cells is a honeycomb made of an aluminum alloy as the whole hierarchical composite cellular structure analyzed in the present paper, leads to [2]

$$\frac{\rho_f^{(i)}}{\rho_s} = \frac{2}{\sqrt{3}} \lambda_f^{(i)}, \qquad i = 1, 2, 3 \tag{A.2}$$

$$\frac{E_f^{(i)}}{E_s} = \frac{4}{\sqrt{3}} \left(\lambda_f^{(i)}\right)^3, \qquad i = 1, 2, 3 \tag{A.3}$$

with $\rho_f^{(i)}$, $E_f^{(i)}$ and ρ_s, E_s, respectively, the density and the Young's modulus of the honeycomb and of the constituent material. Also, $\lambda_f^{(i)}$ is the ratio between the thickness and the length of the cell arms. From (A.2)

$$\lambda_f^{(i)} = \frac{\sqrt{3}}{2} \left(\frac{\rho_f^{(i)}}{\rho_s}\right), \qquad i = 1, 2, 3. \tag{A.4}$$

Substituting (A.4) into (A.3) gives, in view of (A.1),

$$K_w^{(i)} = \frac{4\sqrt{3}}{5} E_s \left(\frac{\rho_f^{(i)}}{\rho_s}\right)^3, \qquad i = 1, 2, 3. \tag{A.5}$$

Finally, from the self-similar condition

$$\rho_f^{(i)} = \rho_f = \alpha\,\rho_s \qquad i = 1, 2, 3 \tag{A.6}$$

and the assumption

$$\lambda_f^{(i)} = \lambda_f, \qquad i = 1, 2, 3, \tag{A.7}$$

follows

$$K_w^{(i)} = K_w = \frac{4\sqrt{3}}{5}\alpha^3\,E_s, \qquad i = 1, 2, 3. \tag{A.8}$$

In particular, assuming $\alpha = 0.4, 0.2, 0.1, 0.05$, (A.8) provides, on order, $K_w = 10^{-1}E_s$, $10^{-2}E_s$, $10^{-3}E_s$, $10^{-4}E_s$.

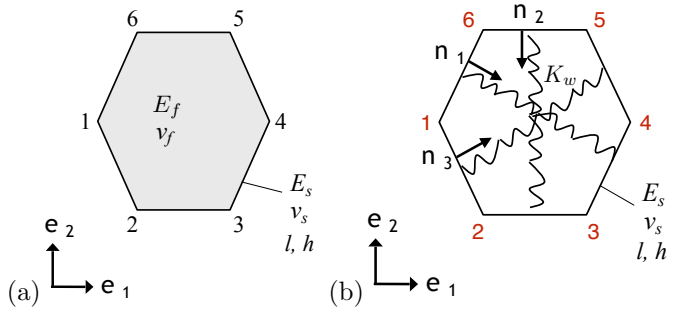

Figure A.1: *Equivalence between the elastic moduli of the filling material and corresponding spring. (a) Filling material as a classical continuum, (b) Filling material as a Winkler foundation.*

Appendix B. A continuum model for composite cellular material with square microstructure

Appendix B.1. Elastic energy

As Figure (B.2a) shows, a sequence of elastic beams of length ℓ forming a periodic array of square cells reproduces a cellular composite material with a square microstructure. Also, an elastic foundation represents the elastic material filling the cells. In particular, the Winkler foundation model simulates each beam, as in [1]. The unit cell of the periodic array (Fig. (B.2b)) is composed by the central node (0) and the four external nodes (1), (2), (3), (4), linked by the elastic beams (0)-(1), (0)-(2), (0)-(3), (0)-(4), represented by the vectors

$$\mathbf{b}_1 = (\ell,\, 0)\,, \qquad \mathbf{b}_2 = (0,\, \ell)\,, \qquad \mathbf{b}_3 = -\mathbf{b}_1, \qquad \mathbf{b}_4 = -\mathbf{b}_2. \tag{B.1}$$

Finally, the area of the unit cell is $A_0 = \ell^2$.

The analysis of the representative cell of the microstructure provides, firstly, the strain energy density of the discrete structure. Its continuum approximation is the consequence of particular assumptions.

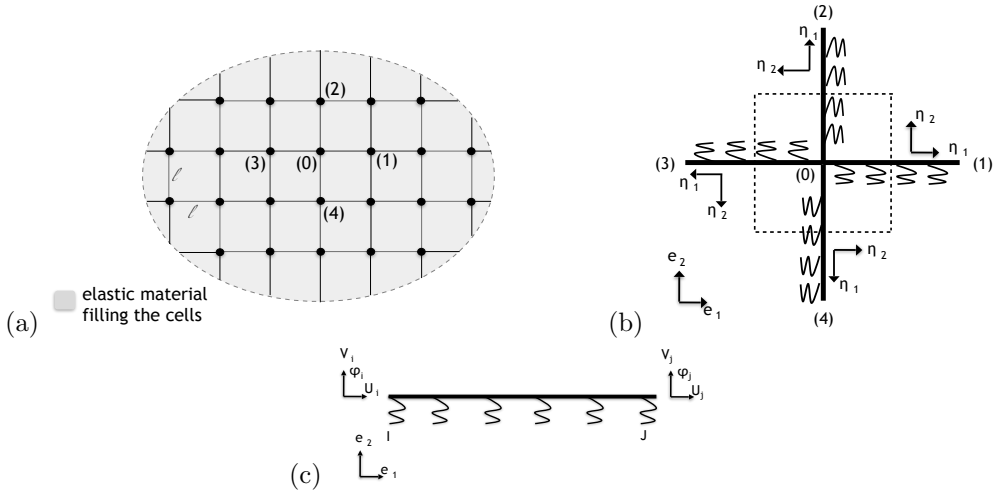

Figure B.2: *(a) The square microstructure, (b) The unit cell, (c) The beam on Winkler elastic foundation.*

First of all, the elastic energy of each beam

$$w^e = \frac{1}{2}(\mathbf{u}^e)^T \cdot \mathbf{k}_b^e \mathbf{u}^e + \frac{1}{2}\left(\frac{1}{2}(\boldsymbol{\Delta}\,\mathbf{u}^{e,a})^T \cdot \mathbf{k}_{wf}^e \boldsymbol{\Delta}\,\mathbf{u}^{e,a}\right) + \frac{1}{2}\left(\frac{1}{2}(\boldsymbol{\Delta}\,\mathbf{u}^{e,b})^T \cdot \mathbf{k}_{wf}^e \boldsymbol{\Delta}\,\mathbf{u}^{e,b}\right), \tag{B.2}$$

derives by superposition principle due to the assumption of linear elastic beam. In particular, $\mathbf{u}^e = [\mathbf{u}_i, \mathbf{u}_j]^T = [u_i, v_i, \varphi_i, u_j, v_j, \varphi_j]^T$ is the generalized *vector of nodal displacement expressed in the local reference* and

$$\boldsymbol{\Delta}\,\mathbf{u}^{e,a} = \left[\boldsymbol{\Delta}\,\mathbf{u}_i^a, \boldsymbol{\Delta}\,\mathbf{u}_j^a\right]^T = \left[\Delta\,u_i^a, \Delta\,v_i^a, \Delta\,\varphi_i^a, \Delta\,u_j^a, \Delta\,v_j^a, \Delta\,\varphi_j^a\right]^T, \tag{B.3}$$

$$\boldsymbol{\Delta}\,\mathbf{u}^{e,b} = \left[\boldsymbol{\Delta}\,\mathbf{u}_i^b, \boldsymbol{\Delta}\,\mathbf{u}_j^b\right]^T = \left[\Delta\,u_i^b, \Delta\,v_i^b, \Delta\,\varphi_i^b, \Delta\,u_j^b, \Delta\,v_j^b, \Delta\,\varphi_j^b\right]^T \tag{B.4}$$

is the elongation of the springs a, the first, and of the springs b, the second (Fig. (B.3)). Note that the factor 1/2 in the second and third term of (B.2), is due to the fact that the springs are shared by two opposite beams and contribute only half of its strain energy to the unit cell. See Appendix D for further details.
The terms $\mathbf{k}_b^e$ and $\mathbf{k}_{wf}^e$ in (B.2) are, respectively, the stiffness matrix of the classical elastic beam and of the Winkler foundation [3], denoted by lowercase letters since they are expressed in the local reference (see [1] for a detailed description). Their components are

$$\mathbf{k}_b^e = \begin{bmatrix} C_\ell/\ell & 0 & 0 & -C_\ell/\ell & 0 & 0 \\ 0 & 12D_\ell/\ell^3 & 6D_\ell/\ell^2 & 0 & -12D_\ell/\ell^3 & 6D_\ell/\ell^2 \\ 0 & 6D_\ell/\ell^2 & 4D_\ell/\ell & 0 & -6D_\ell/\ell^2 & 2D_\ell/\ell \\ -C_\ell/\ell & 0 & 0 & C_\ell/\ell & 0 & 0 \\ 0 & -12D_\ell/\ell^3 & -6D_\ell/\ell^2 & 0 & 12D_\ell/\ell^3 & -6D_\ell/\ell^2 \\ 0 & 6D_\ell/\ell^2 & 2D_\ell/\ell & 0 & -6D_\ell/\ell^2 & 4D_\ell/\ell \end{bmatrix} \tag{B.5}$$

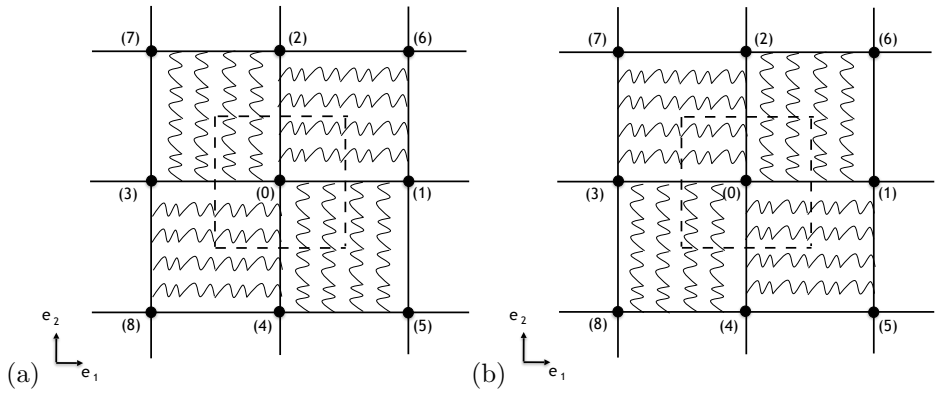

Figure B.3: *Square microstructure: (a) Springs a, (b) Springs b.*

and

$$\mathbf{k}^e_{wf} = \begin{bmatrix} 0 & 0 & 0 & 0 & 0 & 0 \\ 0 & 3\,K_w/35 & 11\,K_w\ell/210 & 0 & 9\,K_w/70 & -13\,K_w\ell/420 \\ 0 & 11\,K_w\ell/210 & K_w\ell^2/105 & 0 & 13\,K_w\ell/420 & -K_w\ell^2/140 \\ 0 & 0 & 0 & 0 & 0 & 0 \\ 0 & 9\,K_w/70 & 13\,K_w\ell/420 & 0 & 13\,K_w/35 & -11\,K_w\ell/210 \\ 0 & -3\,K_w\ell/420 & -K_w\ell^2/140 & 0 & -11\,K_w\ell/210 & K_w\ell^2/105 \end{bmatrix}, \quad \text{(B.6)}$$

with $K_w = k_w\ell$, k_w the Winkler foundation constant per unit width, $C_\ell = \frac{E_s\,h}{1-\nu_s^2}$ and $D_\ell = \frac{E_s\,h^3}{12(1-\nu_s^2)}$, respectively, the tensile and bending stiffness (per unit width) of the beams, h the thickness of the arms, E_s and ν_s the Young's modulus and the Poisson's ratio of the cell walls material.

As it can be seen, the elastic energy is the sum of three terms. The first one,

$$\frac{1}{2}(\mathbf{u}^e)^T \cdot \mathbf{k}^e_b \mathbf{u}^e, \quad \text{(B.7)}$$

corresponding to the classical elastic beam, while the second and the third,

$$\frac{1}{2}\left(\frac{1}{2}(\boldsymbol{\Delta}\,\mathbf{u}^{e,a})^T \cdot \mathbf{k}^e_{wf}\boldsymbol{\Delta}\,\mathbf{u}^{e,a}\right), \qquad \frac{1}{2}\left(\frac{1}{2}(\boldsymbol{\Delta}\,\mathbf{u}^{e,b})^T \cdot \mathbf{k}^e_{wf}\boldsymbol{\Delta}\,\mathbf{u}^{e,b}\right), \quad \text{(B.8)}$$

related to the Winkler foundation and, in particular, to the elongation of the springs a, the first, and of the springs b, the second (Fig. (B.3)).

The elastic energy of the unit cell, W, derives from that of the four beams it consists of. In particular, expressing (B.2) in the global reference and summing the elastic energies of the four beams, leads to

$$W = \frac{W^1 + W^2 + W^3 + W^4}{2}. \quad \text{(B.9)}$$

The presence of the factor 2 in (B.9) is related to the fact that each beam is shared by two adjacent cells. So, each member contributes only half of its strain energy to the representative cell.

The assumption that in the limit $\ell \to 0$ there exist the *continuous displacement and microrotation fields* $\hat{\mathbf{u}}(\cdot)$ and $\hat{\varphi}(\cdot)$, and that the discrete variables previously introduced to represent the degrees of freedom (displacements and rotations) of the external nodes of the unit cell can be expressed by [4]:

$$\mathbf{u}_j = \hat{\mathbf{u}}_0 + \nabla\hat{\mathbf{u}}\,\mathbf{b}_j + \frac{1}{2}\nabla^2\hat{\mathbf{u}}\,\mathbf{b}_j^2, \qquad \varphi_j = \hat{\varphi}_0 + \nabla\hat{\varphi}\,\mathbf{b}_j + \frac{1}{2}\nabla^2\hat{\varphi}\,\mathbf{b}_j^2, \qquad j = 1,2,3,4, \tag{B.10}$$

provides the continuum description of the discrete structure. In (B.10), $\mathbf{b}_j$ are the vectors formerly defined, $\hat{\mathbf{u}}_\mathbf{0}$ and $\hat{\varphi}_0$ are the values of $\hat{\mathbf{u}}(\cdot)$ and $\hat{\varphi}(\cdot)$ at the central point of the cell in the continuum description. The substitution of (B.10) into (B.9) gives the strain energy of the unit cell as a function of the fields $\hat{\mathbf{u}}(\cdot)$ and $\hat{\varphi}(\cdot)$. Finally, dividing the expression that turns out by the area of the unit cell, A_0, leads to the strain energy density in the continuum approximation

$$\begin{aligned} w \;=\; & \frac{C_\ell \ell^2 \left(\varepsilon_{11}^2 + \varepsilon_{22}^2\right) + 24 D_\ell \left(\varepsilon_{12}^2 + (\omega - \hat{\varphi})^2\right) - 2 D_\ell \ell^2 \left(\hat{\varphi}_{,1}^2 + \hat{\varphi}_{,2}^2\right) - 12 D_\ell \ell\, \varepsilon_{12} \hat{\varphi}_{,2}}{2\,\ell^3} + \\ & \frac{K_w \left(210 \left(\varepsilon_{11}^2 + \varepsilon_{22}^2\right) + \ell^2 \left(\hat{\varphi}_{,1}^2 + \hat{\varphi}_{,2}^2\right)\right)}{420}, \end{aligned} \tag{B.11}$$

been $\varepsilon_{\alpha\beta} = \frac{1}{2}\left(\hat{u}_{\alpha,\beta} + \hat{u}_{\beta,\alpha}\right)$ the infinitesimal strains, $\omega = \frac{1}{2}\left(\hat{u}_{1,2} - \hat{u}_{2,1}\right)$ the infinitesimal rotation, $\hat{\varphi}_{,\alpha}$ the microrotation gradients. Note that in (B.11) only the first order derivatives are retained, except for the terms of the form $\hat{\varphi}\,\hat{\varphi}_{,\alpha\alpha}$ that can be integrated by parts and result in first order derivative terms. Retaining this terms, in particular, is important to maintain joint equilibrium, as pointed out in [4], [5], [6].

Moreover, after rewriting (B.11) in terms of $c \equiv C_\ell/\ell = \frac{E_s\,(h/\ell)}{1-\nu_s^2}$ and $d \equiv D_\ell/\ell^3 = \frac{E_s\,(h/\ell)^3}{12(1-\nu_s^2)}$, it emerges that in the resulting energy the coefficients scale with different order in ℓ, as in [7], [1]. Specifically, the microrotation gradients scale with first order in ℓ, while the others coefficients are independent of ℓ. Accordingly, in the limit $\ell \to 0$ the contribution of the microrotation gradients is missing and, as in [1], the equivalent continuum is non-polar. Consequently, the strain energy density in the continuum description is

$$w = \frac{c\left(\varepsilon_{11}^2 + \varepsilon_{22}^2\right) + 24 d \left(\varepsilon_{12}^2 + (\omega - \hat{\varphi})^2\right)}{2\,\ell^3} + \frac{K_w \left(210 \left(\varepsilon_{11}^2 + \varepsilon_{22}^2\right)\right.}{420}. \tag{B.12}$$

Appendix B.2. Constitutive equations

The constitutive equations

$$\sigma = \frac{1}{A_0}\,\frac{\partial W}{\partial \nabla \hat{\mathbf{u}}}, \tag{B.13}$$

with σ the Cauchy-type stress tensor, follows from (B.12).

In particular, it emerges that σ is a non-symmetric tensor and its components are

$$\begin{aligned}
\sigma_{11} &= \sigma_{11}^{sym} = \left(\frac{C_\ell}{\ell} + K_w\right)\varepsilon_{11}, \\
\sigma_{22} &= \sigma_{22}^{sym} = \left(\frac{C_\ell}{\ell} + K_w\right)\varepsilon_{22}, \\
\sigma_{12}^{sym} &= \sigma_{21}^{sym} = \frac{12D_\ell}{\ell^3}\varepsilon_{12}, \\
\sigma_{12}^{skw} &= -\sigma_{21}^{skw} = \frac{12D_\ell}{\ell^3}\left(\omega - \hat{\varphi}\right), \\
\sigma_{12} &= \sigma_{12}^{sym} + \sigma_{12}^{skw}, \quad \sigma_{21} = \sigma_{21}^{sym} + \sigma_{21}^{skw},
\end{aligned} \tag{B.14}$$

with $\sigma_{\gamma\delta}^{sym}$ and $\sigma_{\gamma\delta}^{skw}$, in turn, the symmetric and skew-symmetric parts of σ. See [1] for further details.

Appendix B.3. Elastic constants

Simple mathematical manipulations lead to the elastic constants in the continuum approximation. Specifically, the stress state $\sigma_{11} \neq 0$, $\sigma_{22} = \sigma_{12} = \sigma_{21} = 0$ provide, in view of (B.14) and Hooke's law $\sigma_{11}^{sym} = E_1^* \varepsilon_{11}$, the Young's modulus in the $\mathbf{e_1}$ direction:

$$E_1^* = \frac{\sigma_{11}}{\varepsilon_{11}} = \frac{E_s \lambda}{(1-\nu_s^2)} + K_w, \tag{B.15}$$

with E_s and ν_s, respectively, the Young's modulus and the Poisson's ratio of the cell walls material, $\lambda = h/\ell$ the ratio between the thickness and the length of the beams. The related Poisson's ratio $\nu_{12}^* = -\varepsilon_{22}/\varepsilon_{11}$ is

$$\nu_{12}^* = 0. \tag{B.16}$$

Similarly, the stress state defined as $\sigma_{22} \neq 0$, $\sigma_{11} = \sigma_{12} = \sigma_{21} = 0$ gives the Young's modulus in the $\mathbf{e_2}$ direction:

$$E_2^* = \frac{\sigma_{22}}{\varepsilon_{22}} = \frac{E_s \lambda}{(1-\nu_s^2)} + K_w, \tag{B.17}$$

and the related Poisson's ratio $\nu_{21}^* = -\varepsilon_{11}/\varepsilon_{22} = 0$.

As it can be seen, it emerges that $E_1^* = E_2^* \equiv E^*$ and $\nu_{12}^* = \nu_{21}^* \equiv \nu^*$, with E^* and ν^* stands for the Young's modulus, the first, and the Poisson's ratio, the second, of the approximated continuum.

The tangential elastic modulus, $G^* = \sigma_{12}^{sym}/2\,\varepsilon_{12}$, it is easily obtained by considering the stress state $\sigma_{12}^{sym} \neq 0$, $\sigma_{11} = \sigma_{22} = 0$:

$$G^* = \frac{\sigma_{12}^{sym}}{2\,\varepsilon_{12}} = \frac{E_s \lambda^3}{2\,(1-\nu_s^2)}. \tag{B.18}$$

It should be noted that the elastic moduli derived do not satisfy the classical relation for isotropic materials, $G^* = \dfrac{E^*}{2\,(1+\nu^*)}$. The effective elastic constants are equal only in the $\mathbf{e_1}$ and $\mathbf{e_2}$ direction [2], [8].

Analogous calculations, in conjunction with the classic transformation equations for stress and strain, provide the effective elastic moduli associated with different axis. In particular, denoting with E^*_θ, ν^*_θ, G^*_θ, respectively, the Young's modulus, Poisson's ratio and shear modulus associated with the axis rotated counterclockwise through an angle of θ from ($\mathbf{e_1}$, $\mathbf{e_2}$), it emerges:

$$E^*_\theta = \frac{\lambda^3 E_s (K_w\left(1-\nu_s^2\right)+\lambda E_s)}{(1-\nu_s^2)\left(c^4\lambda^3 E_s+\lambda^3 s^4 E_s+2c^2s^2(K_w\,(1-\nu_s^2)+\lambda E_s)\right)}, \tag{B.19}$$

$$\nu^*_\theta = \frac{2c^2s^2(K_w\left(1-\nu_s^2\right)+\lambda E_s-\lambda^3 E_s)}{c^4\lambda^3 E_s+\lambda^3 s^4 E_s+2c^2s^2(K_w\,(1-\nu_s^2)+\lambda E_s)}, \tag{B.20}$$

$$G^*_\theta = \frac{\lambda^3 E_s (K_w\left(1-\nu_s^2\right)+\lambda E_s)}{4\,(1-\nu_s^2)\left((c^2-s^2)^2 K_w\,(1-\nu_s^2)+\lambda(c^4+2c^2(-1+2\lambda^2)s^2+s^4)E_s\right)}. \tag{B.21}$$

To simplify the notation, c and s stand, respectively, for $\cos\theta$ and $\sin\theta$.

Appendix B.4. Comparison between the analytical and numerical approach

Writing the constitutive equations derived in Section B.2 in a compact way, provide

$$\begin{bmatrix} \sigma_{11}^{sym} \\ \sigma_{22}^{sym} \\ \sigma_{12}^{sym} \end{bmatrix} = \begin{bmatrix} C_{11} & C_{12} & C_{13} \\ C_{21} & C_{22} & C_{23} \\ C_{31} & C_{32} & C_{33} \end{bmatrix} \begin{bmatrix} \varepsilon_{11} \\ \varepsilon_{22} \\ \varepsilon_{12} \end{bmatrix}, \tag{B.22}$$

been

$$\begin{aligned} C_{11} = C_{22} \quad &= \frac{C_\ell}{\ell} + K_w = \frac{E_s\,\lambda}{(1-\nu_s^2)} + K_w, \\ C_{33} \quad &= \frac{12 D_\ell}{\ell^3} = \frac{E_s\,\lambda^3}{(1-\nu_s^2)}, \end{aligned}$$

$$C_{12} = C_{21} = \quad C_{13} = C_{23} = C_{31} = C_{32} = 0. \tag{B.23}$$

In terms of stress,

$$\begin{bmatrix} \varepsilon_{11} \\ \varepsilon_{22} \\ \varepsilon_{12} \end{bmatrix} = \begin{bmatrix} C^*_{11} & C^*_{12} & C^*_{13} \\ C^*_{21} & C^*_{22} & C^*_{23} \\ C^*_{31} & C^*_{32} & C^*_{33} \end{bmatrix} \begin{bmatrix} \sigma_{11}^{sym} \\ \sigma_{22}^{sym} \\ \sigma_{12}^{sym} \end{bmatrix} \tag{B.24}$$

where

$$\begin{aligned} C^*_{11} = C^*_{22} \quad &= \frac{C_{22}\,C_{33}}{C_{22}^2\,C_{33}-C_{12}^2\,C_{33}} = \frac{(1-\nu_s^2)}{K_w(1-\nu_s^2)+E_s\,\lambda}, \\ C^*_{33} \quad &= \frac{C_{22}^2-C_{12}^2}{C_{22}^2\,C_{33}-C_{12}^2\,C_{33}} = \frac{(1-\nu_s^2)}{E_s\,\lambda^3}, \end{aligned}$$

$$C^*_{12} = C^*_{21} = \quad C^*_{13} = C^*_{23} = C^*_{31} = C^*_{32} = 0. \tag{B.25}$$

Finite element simulations on a computational model of the microstructure evaluate the accuracy of the theoretical model. In particular, the Euler-Bernoulli beam on Winkler foundation elements model the composite square microstructure. The cell wall material, isotropic linear elastic for assumption, has Young's modulus $E_s = 79$ GPa, Poisson's ratio $\nu_s = 0.35$ and thickness $h = 0.1\ell$. In terms of Winkler foundation, $K_w = 10^{-2}E_s$. The numerical analysis involve a 50x50 mm square domain discretized in an increasing number of square cells of gradually smaller length ℓ. As done in [1], the load conditions are the uniaxial compression, uniaxial traction and in-plane shear. Specifically, forces of the same intensity acting at the boundary, unconstrained nodes of the domain simulate the loading states. The corresponding effective stiffness components are derived as the ratio between the average volume strain,

$$\overline{\varepsilon}_{ij} = \frac{1}{V}\int_V \varepsilon_{ij}\, dV, \qquad i,j = 1,2, \tag{B.26}$$

and the applied stress. Referring the interested reader to [1] for a comprehensive description, in the case of forces acting horizontally, (B.24) takes the form

$$\overline{\varepsilon}^{(1)} = \begin{bmatrix} \overline{\varepsilon}_{11}^{(1)} \\ \overline{\varepsilon}_{22}^{(1)} \\ \overline{\varepsilon}_{12}^{(1)} \end{bmatrix} = \begin{bmatrix} C_{11}^* & C_{12}^* & C_{13}^* \\ C_{21}^* & C_{22}^* & C_{23}^* \\ C_{31}^* & C_{32}^* & C_{33}^* \end{bmatrix} \begin{bmatrix} \sigma_{11} \\ 0 \\ 0 \end{bmatrix} = \begin{bmatrix} C_{11}^*\sigma_{11} \\ C_{21}^*\sigma_{11} \\ C_{31}^*\sigma_{11} \end{bmatrix}, \tag{B.27}$$

been σ_{11} the applied stress, $\overline{\varepsilon}^{(1)}$ the corresponding strain vector,

$$\overline{\varepsilon}_{ij}^{(1)} = \frac{1}{V}\int_V \varepsilon_{ij}^{(1)}\, dV, \qquad i,j = 1,2, \tag{B.28}$$

and V is the volume of the domain. Accordingly,

$$C_{11}^* = \frac{\overline{\varepsilon}_{11}^{(1)}}{\sigma_{11}}, \qquad C_{21}^* = \frac{\overline{\varepsilon}_{22}^{(1)}}{\sigma_{11}}, \qquad C_{31}^* = \frac{\overline{\varepsilon}_{12}^{(1)}}{\sigma_{11}}, \tag{B.29}$$

Note that the present analysis involve a domain with unitary width, composed by a sequence of discrete beams having the same length ℓ and the same thickness h. Consequently, denoting by s the parametric coordinate along the length of the beam ($0 \le s \le \ell$) and remembering that

$$\varepsilon_{ij}(s) = \frac{1}{2}\left(\frac{\partial u_i(s)}{\partial x_j} + \frac{\partial u_j(s)}{\partial x_i}\right), \tag{B.30}$$

$$\overline{\varepsilon}_{ij}^{(1)} = \frac{\sum_{m=1}^{n_b} \frac{1}{2}\left((u_i(\ell) - u_i(0))\,\frac{\partial s}{\partial x_j} + (u_j(\ell) - u_j(0))\,\frac{\partial s}{\partial x_i}\right)_m}{n_b\,\ell}. \tag{B.31}$$

been n_b the number of the beams. Furthermore, the classical continuum mechanics provides the Young's modulus, E_1^*, and the related Poisson's ratio ν_{12}^*:

$$E_1^* = \frac{\sigma_{11}}{\overline{\varepsilon}_{11}^{(1)}}, \qquad \nu_{12}^* = -\frac{\overline{\varepsilon}_{22}^{(1)}}{\overline{\varepsilon}_{11}^{(1)}}. \tag{B.32}$$

Similarly, when the forces act vertically,

$$\overline{\varepsilon}^{(2)} = \begin{bmatrix} \overline{\varepsilon}_{11}^{(2)} \\ \overline{\varepsilon}_{22}^{(2)} \\ \overline{\varepsilon}_{12}^{(2)} \end{bmatrix} = \begin{bmatrix} C_{11}^* & C_{12}^* & C_{13}^* \\ C_{21}^* & C_{22}^* & C_{23}^* \\ C_{31}^* & C_{32}^* & C_{33}^* \end{bmatrix} \begin{bmatrix} 0 \\ \sigma_{22} \\ 0 \end{bmatrix} = \begin{bmatrix} C_{12}^* \sigma_{22} \\ C_{22}^* \sigma_{22} \\ C_{32}^* \sigma_{22} \end{bmatrix}, \tag{B.33}$$

and, consequently,

$$C_{12}^* = \frac{\overline{\varepsilon}_{11}^{(2)}}{\sigma_{22}}, \qquad C_{22}^* = \frac{\overline{\varepsilon}_{22}^{(2)}}{\sigma_{22}}, \qquad C_{32}^* = \frac{\overline{\varepsilon}_{12}^{(2)}}{\sigma_{22}}. \tag{B.34}$$

Also,

$$E_2^* = \frac{\sigma_{22}}{\overline{\varepsilon}_{22}^{(2)}}, \qquad \nu_{21}^* = -\frac{\overline{\varepsilon}_{11}^{(2)}}{\overline{\varepsilon}_{22}^{(2)}}. \tag{B.35}$$

with σ_{22} the applied stress, $\overline{\varepsilon}^{(2)}$ the corresponding strain vector and $\overline{\varepsilon}_{ij}^{(2)}$ the average volume strain given by (B.26).

Lastly, the shear loading condition provides

$$\overline{\varepsilon}^{(3)} = \begin{bmatrix} \overline{\varepsilon}_{11}^{(3)} \\ \overline{\varepsilon}_{22}^{(3)} \\ \overline{\varepsilon}_{12}^{(3)} \end{bmatrix} = \begin{bmatrix} C_{11}^* & C_{12}^* & C_{13}^* \\ C_{21}^* & C_{22}^* & C_{23}^* \\ C_{31}^* & C_{32}^* & C_{33}^* \end{bmatrix} \begin{bmatrix} 0 \\ 0 \\ \sigma_{12} \end{bmatrix} = \begin{bmatrix} C_{13}^* \sigma_{12} \\ C_{23}^* \sigma_{12} \\ C_{33}^* \sigma_{12} \end{bmatrix}, \tag{B.36}$$

$$C_{13}^* = \frac{\overline{\varepsilon}_{11}^{(3)}}{\sigma_{12}}, \qquad C_{23}^* = \frac{\overline{\varepsilon}_{22}^{(3)}}{\sigma_{12}}, \qquad C_{33}^* = \frac{\overline{\varepsilon}_{12}^{(3)}}{\sigma_{12}}. \tag{B.37}$$

and

$$G^* = \frac{\sigma_{12}}{2\,\overline{\varepsilon}_{12}^{(3)}} \tag{B.38}$$

As before, σ_{12} and $\overline{\varepsilon}^{(3)}$ are, in turn, the applied stress and the corresponding strain vector, while $\overline{\varepsilon}_{ij}^{(3)}$ is the average volume strain defined in (B.26).

Tables (B.1) and (B.2) present the outcome of the present study. In Table (B.1), in particular, the comparison involves the theoretical and numerical C_{ij}^* constants. In Table (B.2), the theoretical and numerical elastic moduli. Both Table (B.1) and Table (B.2) show that the analytical quantities are in accordance with the numerical results.

Appendix C. A continuum model for composite cellular material with equilateral triangular microstructure

Appendix C.1. Elastic energy

As in Appendix B, a sequence of Euler-Bernoulli beams on Winkler foundation elements model the triangular microstructure (Fig. (C.4). As Figure (C.4b) shows, the unit cell of the periodic configuration is composed by the central node (0) and the six external nodes (1), (2), (3), (4), (5), (6), linked by the elastic beams (0)-(1), (0)-(2), (0)-(3), (0)-(4), (0)-(5), (0)-(6), represented by the vectors

$$\begin{aligned} &\mathbf{b}_1 = (\ell,\, 0)\,, \quad \mathbf{b}_2 = \left(\ell/2,\, \sqrt{3}\,\ell/2\right), \quad \mathbf{b}_3 = \left(-\ell/2,\, \sqrt{3}\,\ell/2\right), \\ &\mathbf{b}_4 = -\mathbf{b}_1, \qquad \mathbf{b}_5 = -\mathbf{b}_2, \qquad \mathbf{b}_6 = -\mathbf{b}_3. \end{aligned} \tag{C.1}$$

Table B.1: *Square microstructure: comparison between the analytical and numerical approach, C^*_{ij} constants*

No. cells	ℓ (mm)	C^*_{11}	C^*_{22}	C^*_{33}	$C^*_{12} = C^*_{21} = C^*_{13} = C^*_{23} = C^*_{31} = C^*_{32}$
10x10	5	0.08	0.10	9.39	0
50x50	1	0.10	0.11	10.70	0
100x100	0.5	0.11	0.11	10.70	0
200x200	0.25	0.11	0.11	10.74	0
250x250	0.2	0.11	0.11	10.79	0
400x400	0.125	0.11	0.11	10.82	0
500x500	0.1	0.11	0.11	10.95	0
Analytical results		0.11	0.11	11.11	0

Table B.2: *Square microstructure: comparison between the analytical and numerical approach, elastic moduli*

No. cells	ℓ (mm)	E^*_1 (GPa)	E^*_2 (GPa)	ν^*_{12}	ν^*_{21}	G^* (GPa)
10x10	5	12.50	10.00	0	0	0.09
50x50	1	9.57	9.18	0	0	0.05
100x100	0.5	9.28	9.10	0	0	0.05
200x200	0.25	9.15	9.06	0	0	0.05
250x250	0.2	9.12	9.05	0	0	0.05
400x400	0.125	9.08	9.04	0	0	0.05
500x500	0.1	9.08	9.04	0	0	0.05
Analytical results		9.00	9.00	0	0	0.05

The area of the unit cell is $A_0 = \sqrt{3}\,\ell^2/2$, with ℓ the length of the beams [9], [4]. As before, the elastic energy of each beam is obtained by superposition principle

$$w^e = \frac{1}{2}(\mathbf{u}^e)^T \cdot \mathbf{k}_b^e \mathbf{u}^e + \frac{1}{2}\left(\frac{1}{2}(\boldsymbol{\Delta}\,\mathbf{u}^{e,a})^T \cdot \mathbf{k}_{wf}^e \boldsymbol{\Delta}\,\mathbf{u}^{e,a}\right) + \frac{1}{2}\left(\frac{1}{2}(\boldsymbol{\Delta}\,\mathbf{u}^{e,b})^T \cdot \mathbf{k}_{wf}^e \boldsymbol{\Delta}\,\mathbf{u}^{e,b}\right), \tag{C.2}$$

with $\mathbf{u}^e$, $\boldsymbol{\Delta}\,\mathbf{u}^{e,a}$, $\boldsymbol{\Delta}\,\mathbf{u}^{e,b}$, $\mathbf{k}_b^e$, $\mathbf{k}_{wf}$, in turn, the vector of nodal displacements, the elongation of the two sets of springs and the stiffness matrices previously defined. See Appendix E for further details. The elastic energy of the unit cell, W, derives from that of the six beams it consists of. Note that each beam is shared between two adjacent cells. Consequently, each member contributes only half of its strain energy to the unit cell.

It is not difficult to see that the first node of each beam coincides with the central node (0). So, denoted by $\mathbf{u}_0$ the displacements of the node (0) and by $\boldsymbol{\Delta}\,\mathbf{u}_0^a$, $\boldsymbol{\Delta}\,\mathbf{u}_0^b$ the elongation of the springs in (0), follows $\mathbf{u}_i = \mathbf{u}_0$, $\boldsymbol{\Delta}\,\mathbf{u}_i^a = \boldsymbol{\Delta}\,\mathbf{u}_0^a$ and $\boldsymbol{\Delta}\,\mathbf{u}_i^b = \boldsymbol{\Delta}\,\mathbf{u}_0^b$.

As done in [7], [1], expressing (C.2) in the global reference, adding up forces at the central node (0) and condensing the corresponding degrees of freedom to take account of the forces balance in (0), leads to

$$W = W(\mathbf{u}_j, \boldsymbol{\Delta}\,\mathbf{u}_j^a, \boldsymbol{\Delta}\,\mathbf{u}_j^b), \quad j = 1,2,3,4,5,6. \tag{C.3}$$

The assumption that in the limit $\ell \to 0$ the discrete variables $(\mathbf{u_j}, \varphi_j)$ can be expressed by

$$\mathbf{u}_j = \hat{\mathbf{u}}_0 + \nabla\hat{\mathbf{u}}\,\mathbf{b}_j, \qquad \varphi_j = \hat{\varphi}_0 + \nabla\hat{\varphi}\,\mathbf{b}_j, \qquad j = 1,2,3,4,5,6 \tag{C.4}$$

provides the continuum description of the discrete structure. The terms $\hat{\mathbf{u}}_0$ and $\hat{\varphi}_0$ in (C.4) are the values of $\hat{\mathbf{u}}(\cdot)$ and $\hat{\varphi}(\cdot)$ at the central point of the cell in the continuum description. Substituting (C.4) into (C.3) gives the strain energy of the unit cell as a function of the fields $\hat{\mathbf{u}}$ and $\hat{\varphi}$.

Finally, dividing the expression that turns out from the calculation by the area of the unit cell, A_0, gives the strain energy density in the continuum approximation w:

$$\begin{aligned} w \;=\; & \frac{\sqrt{3}\left(C_\ell^2\ell^4\left(3\varepsilon_{11}^2 + 4\varepsilon_{12}^2 + 2\varepsilon_{11}\varepsilon_{22} + 3\varepsilon_{22}^2\right) + 48C_\ell D_\ell \ell^2\left(\varepsilon_{11}^2 + \varepsilon_{22}^2 + 2\varepsilon_{12}^2\right)\right)}{96D_\ell\ell^3 + 8C_\ell\ell^5} + \\ & \frac{6\sqrt{3}\left(D_\ell^2\left(3\varepsilon_{11}^2 + 12\varepsilon_{12}^2 - 6\varepsilon_{11}\varepsilon_{22} + 3\varepsilon_{22}^2\right) + D_\ell\left(12D_\ell + C_\ell\ell^2\right)(\omega - \hat{\varphi})^2\right)}{12D_\ell\ell^3 + C_\ell\ell^5} + \\ & \frac{2\sqrt{3}\left(D_\ell\ell^2\left(3D_\ell + C_\ell\ell^2\right)\left(\hat{\varphi}_{,1}^2 + \hat{\varphi}_{,2}^2\right)\right)}{12D_\ell\ell^3 + C_\ell\ell^5} + \\ & \frac{K_w\left(39\left(59\varepsilon_{11}^2 + 96\varepsilon_{12}^2 + 22\varepsilon_{11}\varepsilon_{22} + 59\varepsilon_{22}^2\right) + 70\ell^2\left(\hat{\varphi}_{,1}^2 + \hat{\varphi}_{,2}^2\right)\right)}{4480\sqrt{3}} \end{aligned} \tag{C.5}$$

been $C_\ell = \frac{E_s\,h}{1-\nu_s^2}$ and $D_\ell = \frac{E_s\,h^3}{12(1-\nu_s^2)}$, respectively, the tensile and bending stiffness (per unit width) of the beams, h the thickness, E_s and ν_s the Young's modulus and the Poisson's ratio of the cell walls material, $K_w = k_w\ell$, k_w the Winkler foundation constant per unit width. In particular, the resulting energy density

$$w = w\left(\varepsilon_{\alpha\beta}, (\omega - \hat{\varphi}), \hat{\varphi}_{,\alpha}\right) \tag{C.6}$$

is a function of the infinitesimal strains $\varepsilon_{\alpha\beta} = \frac{1}{2}\left(\hat{u}_{\alpha,\beta} + \hat{u}_{\beta,\alpha}\right)$ and the infinitesimal rotation $\omega = \frac{1}{2}\left(\hat{u}_{1,2} - \hat{u}_{2,1}\right)$ that represent, respectively, the symmetric and skew-symmetric part of $\nabla\hat{\mathbf{u}}$, as in the classical continuum mechanics, and of the microrotation gradients, $\hat{\varphi}_{,\alpha}$.

After rewriting (C.5) in terms of $c \equiv C_\ell/\ell = \frac{E_s\,(h/\ell)}{1-\nu_s^2}$ and $d \equiv D_\ell/\ell^3 = \frac{E_s\,(h/\ell)^3}{12(1-\nu_s^2)}$, it emerges, as before, that the coefficients are independent of ℓ, with the exception of the microrotation gradients that scale with first order in ℓ. Consequently, in the limit $\ell \to 0$ the contribution of the microrotation gradients is missing and the equivalent continuum is non-polar. Accordingly, the strain energy density in the continuum approximation takes the form:

$$
\begin{aligned}
w \;=\; & \frac{\sqrt{3}\left(C_\ell^2\ell^4\left(3\varepsilon_{11}^2+4\varepsilon_{12}^2+2\varepsilon_{11}\varepsilon_{22}+3\varepsilon_{22}^2\right)+48C_\ell D_\ell\ell^2\left(\varepsilon_{11}^2+\varepsilon_{22}^2+2\varepsilon_{12}^2\right)\right)}{96D_\ell\ell^3+8C_\ell\ell^5} + \\
& \frac{6\sqrt{3}\left(D_\ell^2\left(3\varepsilon_{11}^2+12\varepsilon_{12}^2-6\varepsilon_{11}\varepsilon_{22}+3\varepsilon_{22}^2\right)+D_\ell\left(12D_\ell+C_\ell\ell^2\right)\left(\omega-\hat{\varphi}\right)^2\right)}{12D_\ell\ell^3+C_\ell\ell^5} + \\
& \frac{K_w\left(39\left(59\varepsilon_{11}^2+96\varepsilon_{12}^2+22\varepsilon_{11}\varepsilon_{22}+59\varepsilon_{22}^2\right)\right)}{4480\sqrt{3}}.
\end{aligned}
\tag{C.7}
$$

Appendix C.2. Constitutive equations

The constitutive equations ensue from (C.7):

$$
\begin{aligned}
\sigma_{11} = \sigma_{11}^{sym} &= \left(\frac{\sqrt{3}\left(3C_\ell\ell^2+12D_\ell\right)}{4\,\ell^3}+\frac{767\,K_w}{2240\sqrt{3}}\right)\varepsilon_{11}+\left(\frac{\sqrt{3}\left(C_\ell\ell^2-12D_\ell\right)}{4\,\ell^3}+\frac{143\,K_w}{2240\sqrt{3}}\right)\varepsilon_{22}, \\
\sigma_{22} = \sigma_{22}^{sym} &= \left(\frac{\sqrt{3}\left(3C_\ell\ell^2+12D_\ell\right)}{4\,\ell^3}+\frac{767\,K_w}{2240\sqrt{3}}\right)\varepsilon_{22}+\left(\frac{\sqrt{3}\left(C_\ell\ell^2-12D_\ell\right)}{4\,\ell^3}+\frac{143\,K_w}{2240\sqrt{3}}\right)\varepsilon_{11}, \\
\sigma_{12}^{sym} = \sigma_{21}^{sym} &= \left(\frac{\sqrt{3}\left(C_\ell\ell^2+12D_\ell\right)}{2\,\ell^3}+\frac{39\,K_w}{140\sqrt{3}}\right)\varepsilon_{12} \\
\sigma_{12}^{skw} = -\sigma_{21}^{skw} &= \frac{12\sqrt{3}\,D_\ell}{\ell^3}\left(\omega-\hat{\varphi}\right), \\
\sigma_{12} = \sigma_{12}^{sym} + \sigma_{12}^{skw}, &\quad \sigma_{21} = \sigma_{21}^{sym} + \sigma_{21}^{skw}.
\end{aligned}
\tag{C.8}
$$

$\sigma_{\gamma\delta}^{sym}$ and $\sigma_{\gamma\delta}^{skw}$ are, in turn, the symmetric and skew-symmetric part of the not-symmetric Cauchy-type stress tensor.

Appendix C.3. Elastic constants

Let us consider the stress state $\sigma_{11} \neq 0$, $\sigma_{22} = \sigma_{12} = \sigma_{21} = 0$. From (C.8) and Hooke's law, $\sigma_{11}^{sym} = E_1^*\,\varepsilon_{11}$, the Young's modulus in the $\mathbf{e_1}$ direction is:

$$
E_1^* = \frac{\sigma_{11}}{\varepsilon_{11}} = \frac{\sqrt{3}\left(13\,K_w(1-\nu_s^2)+32E_s\,\lambda\right)\left(39\,K_w(1-\nu_s^2)+70E_s\,\lambda\left(1+\lambda^2\right)\right)}{2(1-\nu_s^2)\left(767K_w(1-\nu_s^2)+560E_s\,\lambda\,(3+\lambda^2)\right)}, \tag{C.9}
$$

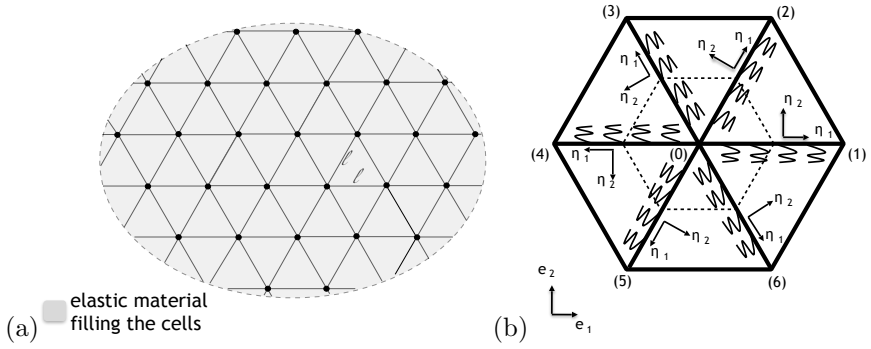

Figure C.4: *(a) The equilateral triangular microstructure, (b) The unit cell.*

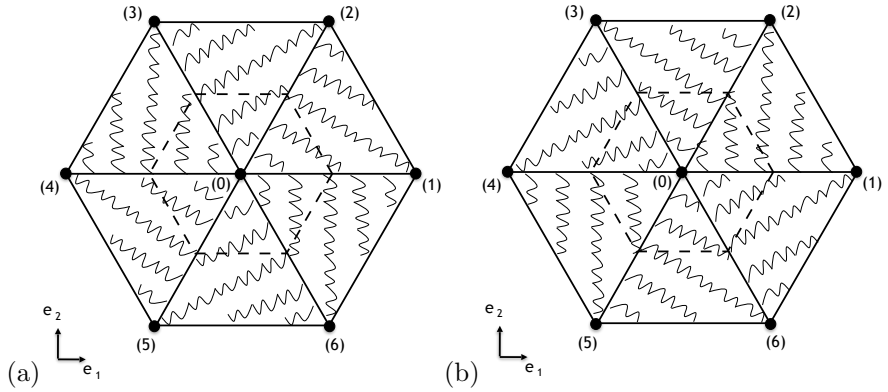

Figure C.5: *Equilateral triangular microstructure: (a) Springs a, (b) Springs b.*

while the related Poisson's ratio $\nu_{12}^* = -\varepsilon_{22}/\varepsilon_{11}$ is:

$$\nu_{12}^* = \frac{143K_w(1-\nu_s^2) - 560_s\left(\lambda^2-1\right)}{767K_w(1-\nu_s^2) + 560_s\left(\lambda^2+3\right)}. \tag{C.10}$$

Similarly, the stress state $\sigma_{22} \neq 0$, $\sigma_{11} = \sigma_{12} = \sigma_{21} = 0$ leads to the Young's modulus in the $\mathbf{e_2}$ direction, $E_2^* = E_1^* \equiv E^*$, and to the related Poisson's ratio, $\nu_{21}^* = -\varepsilon_{11}/\varepsilon_{22} = \nu_{12}^* \equiv \nu^*$.

Finally, the stress state $\sigma_{12}^{sym} \neq 0$, $\sigma_{11} = \sigma_{22} = 0$ yields the tangential elastic modulus, $G^* = \sigma_{12}^{sym}/2\,\varepsilon_{12}$:

$$G^* = \frac{\sqrt{3}\left(39K_w(1-\nu_s^2) + 70_s\left(\lambda^2+1\right)\right)}{280(1-\nu_s^2)}. \tag{C.11}$$

Appendix C.4. Comparison between the analytical and numerical approach

In terms of stress, the compact expression of the constitutive equations derived in Section C.2 is

$$\begin{bmatrix} \varepsilon_{11} \\ \varepsilon_{22} \\ \varepsilon_{12} \end{bmatrix} = \begin{bmatrix} C_{11}^* & C_{12}^* & C_{13}^* \\ C_{21}^* & C_{22}^* & C_{23}^* \\ C_{31}^* & C_{32}^* & C_{33}^* \end{bmatrix} \begin{bmatrix} \sigma_{11}^{sym} \\ \sigma_{22}^{sym} \\ \sigma_{12}^{sym} \end{bmatrix}, \tag{C.12}$$

with

$$\begin{aligned} C_{11}^* = C_{22}^* &= \frac{C_{22}\,C_{33}}{C_{22}^2\,C_{33} - C_{12}^2\,C_{33}}, \qquad C_{12}^* = C_{21}^* = \frac{C_{12}\,C_{33}}{C_{22}^2\,C_{33} - C_{12}^2\,C_{33}}, \\ C_{33}^* &= \frac{C_{22}^2 - C_{12}^2}{C_{22}^2\,C_{33} - C_{12}^2\,C_{33}}, \qquad C_{13}^* = C_{23}^* = C_{31}^* = C_{32}^* = 0. \end{aligned} \tag{C.13}$$

and

$$\begin{aligned} C_{11} = C_{22} &= \frac{\sqrt{3}\left(3C_\ell\ell^2 + 12D_\ell\right)}{4\,\ell^3} + \frac{767\,K_w}{2240\sqrt{3}} = \frac{\sqrt{3}E_s\lambda(3+\lambda^2)}{4(1-\nu_s^2)} + \frac{767\,K_w}{2240\sqrt{3}}, \\ C_{12} = C_{21} &= \frac{\sqrt{3}\left(C_\ell\ell^2 - 12D_\ell\right)}{4\,\ell^3} + \frac{143\,K_w}{2240\sqrt{3}} = \frac{\sqrt{3}E_s\lambda(3-\lambda^2)}{4(1-\nu_s^2)} + \frac{143\,K_w}{2240\sqrt{3}}, \\ C_{33} &= \frac{\sqrt{3}\left(C_\ell\ell^2 + 12D_\ell\right)}{2\,\ell^3} + \frac{39\,K_w}{140\sqrt{3}} = \frac{\sqrt{3}E_s\lambda^3}{(1-\nu_s^2)}, \\ C_{13} = C_{23} = &\quad C_{31} = C_{32} = 0. \end{aligned} \tag{C.14}$$

As in Appendix B, finite element simulations assess the analytical model. Specifically, the Euler-Bernoulli beam on Winkler foundation elements model the composite microstructure. The cell wall material, assumed to be isotropic linear elastic, has Young's modulus $E_s = 79$ GPa, Poisson's ratio $\nu_s = 0.35$ and thickness $h = 0.1\ell$, while $K_w = 10^{-2}E_s$. The numerical analysis involve a 75x50 mm rectangular domain discretized in an increasing number of equilateral triangular cells having gradually smaller length ℓ. As in Appendix B, the load conditions are the uniaxial compression, uniaxial traction and in-plane shear. Forces of the same intensity acting at the boundary, unconstrained nodes of the domain simulate the loading states. Again, the corresponding

Table C.3: *Equilateral triangular microstructure: comparison between the analytical and numerical approach, C^*_{ij} constants*

No. cells	ℓ (mm)	C^*_{11}	C^*_{22}	C^*_{12}	C^*_{21}	C^*_{33}	$C^*_{13} = C^*_{23} = C^*_{31} = C^*_{32}$
15x10	5	6.05	6.08	6.02	6.03	7.50	0
75x50	1	6.13	6.13	6.03	6.03	5.90	0
100x100	0.5	6.25	6.23	6.03	6.05	5.90	0
300x200	0.25	6.27	6.29	6.10	6.09	5.10	0
375x250	0.2	6.35	6.34	6.15	6.13	4.80	0
600x400	0.125	6.38	6.39	6.22	6.21	4.60	0
750x500	0.1	6.38	6.39	6.22	6.22	4.60	0
Analytical results		6.43	6.43	6.40	6.40	4.50	0

Table C.4: *Equilateral triangular microstructure: comparison between the analytical and numerical approach, elastic moduli*

No. cells	ℓ (mm)	E^*_1 (GPa)	E^*_2 (GPa)	ν^*_{12}	ν^*_{21}	G^* (GPa)
15x10	5	11.33	11.48	0.42	0.45	4.70
75x50	1	11.33	11.39	0.41	0.40	4.63
100x100	0.5	11.10	11.08	0.41	0.40	4.63
300x200	0.25	10.91	10.90	0.32	0.33	4.51
375x250	0.2	10.70	10.78	0.33	0.33	4.50
600x400	0.125	10.61	10.50	0.33	0.33	4.22
750x500	0.1	10.50	10.47	0.33	0.33	4.10
Analytical results		10.46	10.46	0.33	0.33	3.94

effective stiffness components are calculated as the ratio between the average volume strain,

$$\overline{\varepsilon}_{ij} = \frac{1}{V}\int_V \varepsilon_{ij}\, dV, \qquad i,j = 1,2, \tag{C.15}$$

and the applied stress (see Appendix B).

The results of the analysis are presented in Tables (C.3) and (C.4). In Table (C.3) the analytical and numerical values of the C^*_{ij} constants are compared, while Table (C.4) deals with the elastic constants. As it can be seen, the results from the continuum formulation compare reasonably well with the numerical solutions.

Appendix D. The composite cellular material with square microstructure: focus on springs

As Figure (D.6) shows, the elongation of the elastic springs is expressed by

- Beam (0)-(1)

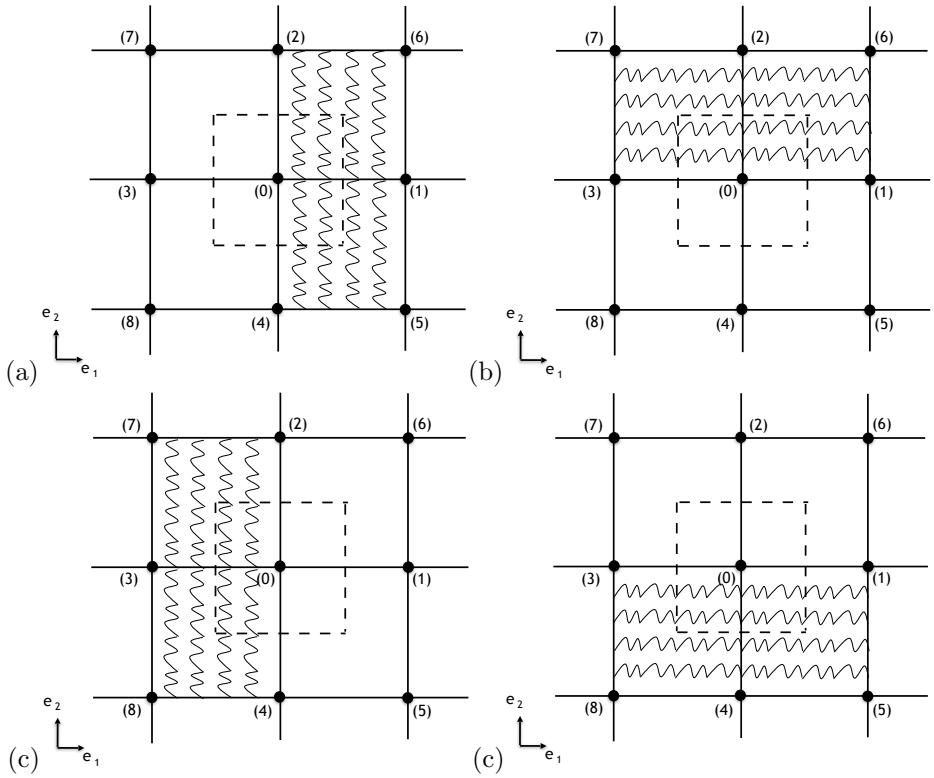

Figure D.6: *The unit cell with focus on springs in the square microstructure. (a) Beam (0)-(1), (b) Beam (0)-(2), (c) Beam (0)-(3), (d) Beam (0)-(4).*

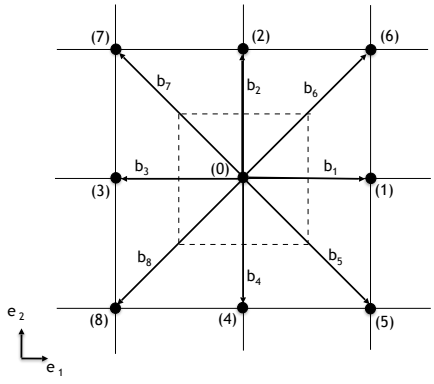

Figure D.7: *The* $\mathbf{b}_i$ *vectors in the square microstructure.*

In the discrete system

$$\boldsymbol{\Delta}\,\mathbf{u}^{1,a} = \begin{bmatrix} \mathbf{u}_0 - \mathbf{u}_4 \\ \varphi_0 - \varphi_4 \\ \mathbf{u}_1 - \mathbf{u}_5 \\ \varphi_1 - \varphi_5 \end{bmatrix}, \quad \boldsymbol{\Delta}\,\mathbf{u}^{1,b} = \begin{bmatrix} \mathbf{u}_0 - \mathbf{u}_2 \\ \varphi_0 - \varphi_2 \\ \mathbf{u}_1 - \mathbf{u}_6 \\ \varphi_1 - \varphi_6 \end{bmatrix}, \tag{D.1}$$

while in the continuum description

$$\mathbf{u}_0 = \hat{\mathbf{u}}, \qquad \varphi_0 = \hat{\varphi}, \tag{D.2}$$

$$\mathbf{u}_i = \hat{\mathbf{u}} + \nabla\hat{\mathbf{u}}\,\mathbf{b}_i + \frac{1}{2}(\nabla^2\hat{\mathbf{u}}\,\mathbf{b}_i^2), \tag{D.3}$$

$$\varphi_i = \hat{\varphi} + \nabla\hat{\varphi}\,\mathbf{b}_i + \frac{1}{2}(\nabla^2\hat{\varphi}\,\mathbf{b}_i^2), \quad i = 1, 2, 4, 5, 6. \tag{D.4}$$

Substituting (D.2)-(D.10) into (D.1) leads to

$$\boldsymbol{\Delta}\,\mathbf{u}^{1,a} = \begin{bmatrix} -\nabla\hat{\mathbf{u}}\,\mathbf{b}_4 - (\nabla^2\hat{\mathbf{u}}\,\mathbf{b}_4^2)/2 \\ -\nabla\hat{\varphi}\,\mathbf{b}_4 - (\nabla^2\hat{\varphi}\,\mathbf{b}_4^2)/2 \\ \nabla\hat{\mathbf{u}}\,\mathbf{b}_1 + (\nabla^2\hat{\mathbf{u}}\,\mathbf{b}_1^2)/2 - \nabla\hat{\mathbf{u}}\,\mathbf{b}_5 - (\nabla^2\hat{\mathbf{u}}\,\mathbf{b}_5^2)/2 \\ \nabla\hat{\varphi}\,\mathbf{b}_1 + (\nabla^2\hat{\varphi}\,\mathbf{b}_1^2)/2 - \nabla\hat{\varphi}\,\mathbf{b}_5 - (\nabla^2\hat{\varphi}\,\mathbf{b}_5^2)/2 \end{bmatrix}, \tag{D.5}$$

$$\boldsymbol{\Delta}\,\mathbf{u}^{1,b} = \begin{bmatrix} -\nabla\hat{\mathbf{u}}\,\mathbf{b}_2 - (\nabla^2\hat{\mathbf{u}}\,\mathbf{b}_2^2)/2 \\ -\nabla\hat{\varphi}\,\mathbf{b}_2 - (\nabla^2\hat{\varphi}\,\mathbf{b}_2^2)/2 \\ \nabla\hat{\mathbf{u}}\,\mathbf{b}_1 + (\nabla^2\hat{\mathbf{u}}\,\mathbf{b}_1^2)/2 - \nabla\hat{\mathbf{u}}\,\mathbf{b}_6 - (\nabla^2\hat{\mathbf{u}}\,\mathbf{b}_6^2)/2 \\ \nabla\hat{\varphi}\,\mathbf{b}_1 + (\nabla^2\hat{\varphi}\,\mathbf{b}_1^2)/2 - \nabla\hat{\varphi}\,\mathbf{b}_6 - (\nabla^2\hat{\varphi}\,\mathbf{b}_6^2)/2 \end{bmatrix}. \tag{D.6}$$

Similarly, for the beams (0)-(2), (0)-(3), (0)-(4):
- Beam (0)-(j)
Discrete system

$$\boldsymbol{\Delta}\,\mathbf{u}^{j,a} = \begin{bmatrix} \mathbf{u}_0 - \mathbf{u}_k \\ \varphi_0 - \varphi_k \\ \mathbf{u}_2 - \mathbf{u}_l \\ \varphi_2 - \varphi_l \end{bmatrix}, \quad \boldsymbol{\Delta}\,\mathbf{u}^{j,b} = \begin{bmatrix} \mathbf{u}_0 - \mathbf{u}_m \\ \varphi_0 - \varphi_m \\ \mathbf{u}_2 - \mathbf{u}_n \\ \varphi_2 - \varphi_n \end{bmatrix}. \tag{D.7}$$

Continuum description

$$\mathbf{u}_0 = \hat{\mathbf{u}}, \qquad \varphi_0 = \hat{\varphi}, \tag{D.8}$$

$$\mathbf{u}_i = \hat{\mathbf{u}} + \nabla\hat{\mathbf{u}}\,\mathbf{b}_i + \frac{1}{2}(\nabla^2\hat{\mathbf{u}}\,\mathbf{b}_i^2), \tag{D.9}$$

$$\varphi_i = \hat{\varphi} + \nabla\hat{\varphi}\,\mathbf{b}_i + \frac{1}{2}(\nabla^2\hat{\varphi}\,\mathbf{b}_i^2), \quad i = j, k, l, m, n \tag{D.10}$$

and

$$\boldsymbol{\Delta}\,\mathbf{u}^{j,a} = \begin{bmatrix} -\nabla\hat{\mathbf{u}}\,\mathbf{b}_k - (\nabla^2\hat{\mathbf{u}}\,\mathbf{b}_k^2)/2 \\ -\nabla\hat{\varphi}\,\mathbf{b}_k - (\nabla^2\hat{\varphi}\,\mathbf{b}_k^2)/2 \\ \nabla\hat{\mathbf{u}}\,\mathbf{b}_j + (\nabla^2\hat{\mathbf{u}}\,\mathbf{b}_j^2)/2 - \nabla\hat{\mathbf{u}}\,\mathbf{b}_l - (\nabla^2\hat{\mathbf{u}}\,\mathbf{b}_l^2)/2 \\ \nabla\hat{\varphi}\,\mathbf{b}_j + (\nabla^2\hat{\varphi}\,\mathbf{b}_j^2)/2 - \nabla\hat{\varphi}\,\mathbf{b}_l - (\nabla^2\hat{\varphi}\,\mathbf{b}_l^2)/2 \end{bmatrix}, \tag{D.11}$$

$$\boldsymbol{\Delta}\,\mathbf{u}^{j,b} = \begin{bmatrix} -\nabla\hat{\mathbf{u}}\,\mathbf{b}_m - (\nabla^2\hat{\mathbf{u}}\,\mathbf{b}_m^2)/2 \\ -\nabla\hat{\varphi}\,\mathbf{b}_m - (\nabla^2\hat{\varphi}\,\mathbf{b}_m^2)/2 \\ \nabla\hat{\mathbf{u}}\,\mathbf{b}_j + (\nabla^2\hat{\mathbf{u}}\,\mathbf{b}_j^2)/2 - \nabla\hat{\mathbf{u}}\,\mathbf{b}_n - (\nabla^2\hat{\mathbf{u}}\,\mathbf{b}_n^2)/2 \\ \nabla\hat{\varphi}\,\mathbf{b}_j + (\nabla^2\hat{\varphi}\,\mathbf{b}_j^2)/2 - \nabla\hat{\varphi}\,\mathbf{b}_n - (\nabla^2\hat{\varphi}\,\mathbf{b}_n^2)/2 \end{bmatrix}. \tag{D.12}$$

In particular,
Beam (0)-(2): $j=2$, $k=1$, $l=6$, $m=3$, $n=7$,
Beam (0)-(3): $j=3$, $k=2$, $l=7$, $m=4$, $n=8$,
Beam (0)-(4): $j=4$, $k=3$, $l=8$, $m=1$, $n=5$.

Finally, the vectors $\mathbf{b}_i$ (Fig. (D.7)) are

$$\begin{array}{llll} \mathbf{b}_1 = (\ell, 0)\,, & \mathbf{b}_2 = (0, \ell)\,, & \mathbf{b}_3 = (-\ell, 0)\,, & \mathbf{b}_4 = (0, -\ell)\,, \\ \mathbf{b}_5 = (\ell, -\ell)\,, & \mathbf{b}_6 = (\ell, \ell)\,, & \mathbf{b}_7 = (-\ell, \ell)\,, & \mathbf{b}_8 = (-\ell, -\ell)\,. \end{array} \tag{D.13}$$

Appendix E. Composite cellular material with equilateral triangular microstructure: focus on springs

In the case of equilateral triangular microstructure, the elongation of the springs takes the form (Fig. (E.8), (E.9))

- Beam (0)-(1)
Discrete system

$$\boldsymbol{\Delta}\,\mathbf{u}_1^a = \begin{bmatrix} \mathbf{u}_1 - \mathbf{u}_6 \\ \varphi_1 - \varphi_6 \end{bmatrix}, \quad \boldsymbol{\Delta}\,\mathbf{u}_1^b = \begin{bmatrix} \mathbf{u}_1 - \mathbf{u}_2 \\ \varphi_1 - \varphi_2 \end{bmatrix}. \tag{E.1}$$

In the continuum description,

$$\mathbf{u}_i = \hat{\mathbf{u}} + \nabla\hat{\mathbf{u}}\,\mathbf{b}_i, \quad \varphi_i = \hat{\varphi} + \nabla\hat{\varphi}\,\mathbf{b}_i, \quad i = 1, 6, 2 \tag{E.2}$$

that, substituted in (E.1), lead to

$$\boldsymbol{\Delta}\,\mathbf{u}_1^a = \begin{bmatrix} \nabla\hat{\mathbf{u}}\,\mathbf{b}_1 - \nabla\hat{\mathbf{u}}\,\mathbf{b}_6 \\ \nabla\hat{\varphi}\,\mathbf{b}_1 - \nabla\hat{\varphi}\,\mathbf{b}_6 \end{bmatrix}, \quad \boldsymbol{\Delta}\,\mathbf{u}_1^b = \begin{bmatrix} \nabla\hat{\mathbf{u}}\,\mathbf{b}_1 - \nabla\hat{\mathbf{u}}\,\mathbf{b}_2 \\ \nabla\hat{\varphi}\,\mathbf{b}_1 - \nabla\hat{\varphi}\,\mathbf{b}_2 \end{bmatrix}. \tag{E.3}$$

For the other beams, similar calculations provide
- Beam (0)-(j)
Discrete system

$$\boldsymbol{\Delta}\,\mathbf{u}_j^a = \begin{bmatrix} \mathbf{u}_j - \mathbf{u}_k \\ \varphi_j - \varphi_k \end{bmatrix}, \quad \boldsymbol{\Delta}\,\mathbf{u}_j^b = \begin{bmatrix} \mathbf{u}_j - \mathbf{u}_l \\ \varphi_j - \varphi_l \end{bmatrix}. \tag{E.4}$$

Continuum description

$$\mathbf{u}_i = \hat{\mathbf{u}} + \nabla\hat{\mathbf{u}}\,\mathbf{b}_i, \quad \varphi_i = \hat{\varphi} + \nabla\hat{\varphi}\,\mathbf{b}_i, \quad i = j, k, l \tag{E.5}$$

and

$$\boldsymbol{\Delta}\,\mathbf{u}_j^a = \begin{bmatrix} \nabla\hat{\mathbf{u}}\,\mathbf{b}_j - \nabla\hat{\mathbf{u}}\,\mathbf{b}_k \\ \nabla\hat{\varphi}\,\mathbf{b}_j - \nabla\hat{\varphi}\,\mathbf{b}_k \end{bmatrix}, \quad \boldsymbol{\Delta}\,\mathbf{u}_j^b = \begin{bmatrix} \nabla\hat{\mathbf{u}}\,\mathbf{b}_j - \nabla\hat{\mathbf{u}}\,\mathbf{b}_l \\ \nabla\hat{\varphi}\,\mathbf{b}_j - \nabla\hat{\varphi}\,\mathbf{b}_l \end{bmatrix}, \tag{E.6}$$

with

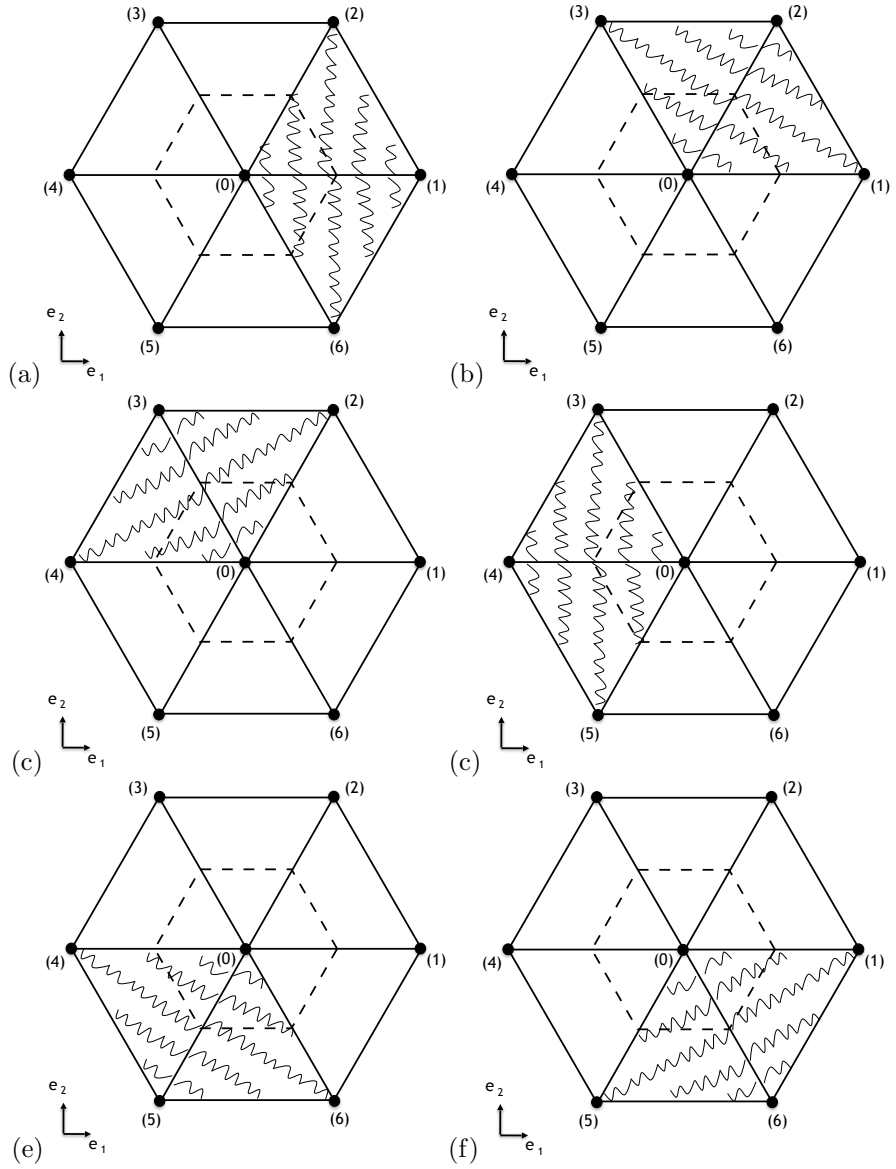

Figure E.8: *The unit cell with focus on springs in the equilateral triangular microstructure. (a) Beam (0)-(1), (b) Beam (0)-(2), (c) Beam (0)-(3), (d) Beam (0)-(4), (e) Beam (0)-(5), (f) Beam (0)-(6).*

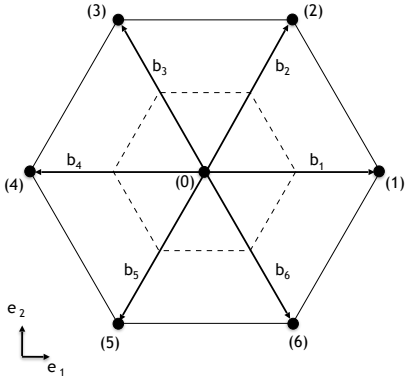

Figure E.9: *The* $\mathbf{b}_i$ *vectors in the equilateral triangular microstructure.*

Beam (0)-(2): $j = 2$, $k = 1$, $l = 3$,
Beam (0)-(3): $j = 3$, $k = 2$, $l = 4$,
Beam (0)-(4): $j = 4$, $k = 3$, $l = 5$,
Beam (0)-(5): $j = 5$, $k = 4$, $l = 6$,
Beam (0)-(6): $j = 6$, $k = 5$, $l = 1$.

Finally, as stated, note that each beam is shared between two adjacent beams. So, each member contributes only half of its strain energy to the representative cell.

References

[1] Ongaro, F., De Falco, P., Pugno, N. M., Barbieri, E., Mechanics of filled cellular materials, *Mech. Mater.*, vol. 97, pp. 26-47, 2016.

[2] Gibson, L. J., Ashby, M. F., Harley, B. A., *Cellular Materials in Nature and Medicine*, Cambridge University Press , 2010.

[3] Janco, R, Solution Methods for Beam and Frames on Elastic Foundation Using the Finite Element Method, *Mechanical Structures and Foundation Engineering*, International scientific conference MSFE 2010.

[4] Kumar, R. S., McDowell, D. L., Generalized continuum modeling of 2-D periodic cellular solids, *Int. J. Solids Struct.*, vol. 41, pp. 7399-7422, 2004.

[5] Bazant, Z. P., Micropolar medium as model for buckling of grid frameworks, *Proceedings of the 12th Midwestern Mechanics Conference*, vol. 6, pp. 587-594, 1971.

[6] Bazant, Z. P., Christensen, M., Analogy between micropolar continuum and grid frameworks under initial stress, *Int. J. Solids Struct.*, vol. 8, pp. 327-346, 1972.

[7] Davini, C., Ongaro, F., A Homogenized Model for Honeycomb cellular materials, *J. Elasticity*, vol. 104, pp. 205-226, 2011.

[8] Arabnejad, S., Pasini, D., Mechanical properties of lattice materials via asymptotic homogenization and comparison with alternative homogenization methods, *International Journal of Mechanical Sciences*, vol. 77, pp. 294-262, 2013.

[9] Chen, J. Y., Huang, Y., Ortiz, M., Fracture analysis of cellular materials: a strain gradient model, *J. Mech. Phys. Solids*, vol. 46, No. 5, pp. 789-828, 1998.